doi:10.1016/j.mseb.2010.02.024

# Chemical vapor deposition of silicon nanodots on $TiO_2$ submicronic powders in vibrated fluidized bed

L. Cadoret [a], C. Rossignol [b,1], J. Dexpert-Ghys [b], B. Caussat [a,*]

[a] *Laboratoire de Génie Chimique, UMR CNRS 5503, Université de Toulouse, ENSIACET/INPT, 4 allée Emile Monso, BP 74233, 31432 Toulouse Cedex 4, France*
[b] *CEMES, UPR CNRS 8011, UPS-Toulouse, 29 rue Jean Marvig, 31055 Toulouse Cedex 4, France*

*Keywords:*
Chemical vapor deposition
Titanium dioxide
Silicon
Transmission electron microscopy
Raman spectroscopy
Infra-red spectroscopy

Silicon nanodots have been deposited on $TiO_2$ submicronic powders in a vibrated fluidized bed chemical vapor deposition (FBCVD) reactor from silane $SiH_4$. Deposition conditions involving very low deposition rates have been studied. After treatment, powders are under the form of micronic agglomerates. In the operating range tested, this agglomerates formation mainly depends on the fluidization conditions and not on the CVD parameters. The best results have been obtained for anatase $TiO_2$ powders for which the conditions of fluidization have been the most optimized. For these anatase powders, agglomerates are porous. SEM and TEM imaging prove that silicon nanodots (8–10 nm in size) have been deposited on the surface of particles and that this deposition is uniform on the whole powders and conformal around each grain, even if not fully continuous. Raman spectroscopy shows that the $TiO_2$ powders have been partially reduced into $TiO_{2-x}$ during deposition. The $TiO_2$ stoichiometry can be recovered by annealing under air, and IR spectroscopy indicates that the deposited silicon nanodots have been at least partly oxidized into $SiO_2$ after this annealing.

## 1. Introduction

The control of the surface properties of micro and nanoparticles is a great challenge since the performances of these particles for many applications could be thus highly enhanced [1,2]. One of the most efficient technologies to coat the outer surface of powders is the fluidized bed chemical vapor deposition (FBCVD) process. CVD offers several advantages compared to wet preparation routes, in particular the absence of solvent and of additional steps of calcination or separation [3]. The fluidized bed (FB) provides incentives for powders coating due to intense solid mixing, excellent heat and mass transfer and homogeneous temperatures [4–6].

However, most literature FBCVD studies concern Geldart's group A or B particles [7], of diameters comprised between 50 and 300 μm, because they are easy to fluidize. For micro and nanometric powders belonging to Geldart's group C, the interparticle cohesive forces are often much greater than the drag forces exerted by the fluid. Consequently, these particles tend to agglomerate, and when subjected to fluidization, they form channels and slugs and do not fluidize individually.

It is possible to partly overcome this problem by activating the fluidization process. Some authors [8–10] propose to improve fluidization by using mechanical stirrers inside the bed or introducing a small amount of large particles into the fine powders. Other groups of searchers [11–13] have shown that mechanical vibrations increase the forces acting on particles and tend to break up agglomerates: the average size of agglomerates is thus reduced and more convenient fluidization behaviors can be obtained.

Only a few works of the literature deal with FBCVD on micronic or submicronic powders. Morooka et al. [14] have deposited TiN on $Si_3N_4$ particles of mean diameter equal to 130 nm, fluidized under the form of agglomerates of 70–700 μm. No indication about the fluidization is given or about the deposition thickness and uniformity. $SnO_2$ from $SnCl_4$ and $H_2O$ has been deposited by FBCVD on ultra fine alumina $Al_2O_3$ particles by Li and Hua [15]. According to these authors, this powder naturally fluidizes under the form of agglomerates. After CVD, $SnO_2$ coated $Al_2O_3$ composite agglomerates were av. 30 μm and were harder than those naturally formed in bed without CVD. But they were easily disintegrated by fingertips. Hakim et al. [16] claim to have conformally coated zirconia particles, 26 nm in diameter, by alumina nanolayers using atomic layer deposition (ALD) in a vibrated fluidized bed (FB) under reduced pressure. Due to their small size, these $ZrO_2$ nanoparticles have been fluidized as aggregates of several hundreds of microns in size. But according to the authors, a dynamic aggregation mechanism has been observed when interparticles forces were minimized in the vibrated FB. These dynamic aggregates partially break apart and

* Corresponding author. Tel.: +33 5 34 32 36 32; fax: +33 5 34 32 37 00.
*E-mail address:* Brigitte.Caussat@ensiacet.fr (B. Caussat).
[1] Permanent address: LEPMI, UJF Grenoble 1, LEPMI, 1130, rue de la Piscine BP 75 38402 – Saint-Martin d'Hères Cedex, France.

reform all along the deposition process, which allows the entire surface of the particles to be exposed to the reactive gases. The same group has deposited in a similar mode iron oxide on zirconia nanoparticles [2], and also alumina nanolayers on various nanopowders including BN platelets, carbon nanotubes, $TiO_2$ and polymeric particles, by ALD into a mechanically stirred FB under reduced pressure [2]. ALD is a self-limiting vapor phase chemisorption process that utilizes critical purge steps to prevent reactions between precursors [16]. CVD is clearly a simpler process.

In the present work, $TiO_2$ submicronic particles have been treated by CVD in a vibrated fluidized bed in order to individually coat each grain by nanometric silicon layers. The aim of such layers is to quench the photocatalytic activity of $TiO_2$ by an inert coating for applications related to pigments and UV blockers in sunscreens [17]. Silane $SiH_4$ has been used as silicon precursor. The influence of the operating conditions on the deposition features has been studied. In particular, the final diameter distribution of powders has been measured by sieving and by laser granulometry, the chemical composition of the deposition has been analyzed by Raman and Infra-red spectroscopy, and its localization on the surface of grains has been evaluated by SEM and TEM imaging.

## 2. Experimental

As detailed elsewhere [18], the FBCVD reactor was made of a vertical cylindrical column of stainless steel with an internal diameter of 0.052 m and a height of 0.8 m. It was externally heated by a three-zone electrical furnace and the wall temperatures were monitored by three thermocouples. Several thermocouples were also placed into a vertical tube of 6 mm in diameter inside the reactor. An Inconel™ porous plate was used for the gas distribution. Electronic grade silane and N50 nitrogen (from Air Liquide) were supplied to the bottom of the bed through ball rotameters connected to manometers. Uncertainties of ±5% could affect the flow rates measured and then the amounts of injected silane. In order to avoid any premature decomposition of silane, the region under the distributor was maintained below 350 °C. A differential fast response pressure sensor (Druck LPX5480) measured the total pressure drop across the bed. The hydrogen concentration of the outlet gases was measured by a catharometer (Hydros100, Rosemount). A DasyLab® system enabled the on-line acquisition of the differential pressure, hydrogen concentration and FB temperatures.

The granular materials used in this study were two groups of nonporous titanium oxide $TiO_2$ particles, one belonging to the anatase crystalline phase (purchased from Sigma–Aldrich), and the other to the rutile phase (from Produits Chimiques du Midi). These two materials have been studied in order to test the ability of our process to treat varied micronic powders; the choice of the crystalline phase was imposed by the purchaser. Their mean volume diameters were respectively 1.6 and 0.52 μm for anatase and rutile $TiO_2$ (0.7 and 0.48 μm for the mean Sauter diameters) as measured by laser granulometry. Their grain density was measured by Helium pycnometry and was equal to 3800 kg/m$^3$; their specific surface areas were equal to 10.07 and 16.3 m$^2$/g respectively, as measured by BET. Their Hausner ratios were equal to 1.86 and 1.5 respectively, classifying both of them into the Geldart's group C.

Their fluidization without vibration was impossible: some gas channels or fixed paths appeared through the bed, which remained quasi-immobile for the whole range of velocities tested. Vibration was then mandatory to overcome the important interparticles forces existing in these beds. The hydrodynamic behavior of the vibrated FB was analyzed by classically measuring the pressure drop of the gas crossing the bed and the bed expansion, as a function of gas velocity [19]. After a long and rigorous study, some convenient fluidization conditions were found for the anatase $TiO_2$ particles, in terms of weight of powders treated per run, type of distributor, frequency and amplitude of vibrations and fluidization velocity, as detailed elsewhere [20]. These optimized conditions of fluidization were also used for the rutile powders.

The deposition conditions tested are detailed in Table 1. The inlet molar fractions of silane and the temperatures were chosen in order to work in conditions of high chemical limitation, i.e. in conditions for which the heterogeneous reaction rate is low in comparison with the gaseous species transport, in order to exalt gaseous species diffusion and to limit external densification of agglomerates due to silicon deposition. The aim was also to deposit very low amounts of Si to form nanometric layers around each grain. The inlet volume percentage of silane was always lower than 4%, and the mean FB temperature did not exceed 595 °C. Rutile $TiO_2$ runs were the first ones to be performed with very low inlet percentages of silane; however, as detailed later, the amount of Si deposited was too low to be detected by TEM. This is why higher silane percentages were used for the anatase runs. Two runs (A4 and A7) were performed using sequential injections of silane, involving a constant flow rate of nitrogen and a slightly variable total flow rate (+ or −2%) due to the $SiH_4$ sequential injections. The duration of each sequence was calculated to obtain a theoretical thickness of 0.5 nm on each grain at each sequence. The total number of sequences was determined in order to inject a total weight of silicon similar to that of runs A1 and A5. The aim was to limit the agglomeration phenomenon in decreasing the surface reactivity of powders during the purges with nitrogen. As a consequence, three modes of silane injection were tested for a similar total weight of silicon injected (runs A1, A4/A7 and A5): for run A1, silane has been injected continuously during 60 min; for run A5 the duration of the experiment was twice, and the inlet fraction of silane was divided per two, to analyze the influence of run duration and of the inlet silane percentage. The influence of deposit temperature was investigated through runs A1,

**Table 1**
Operating conditions tested.

| Run | Temperature gradient before silane injection (°C/cm) | Mean temperature (°C) | Total gas flow rate (nl/h) | Inlet vol. % of $SiH_4$ | Mass of silicon injected (g) | Deposition duration (min) | Injection mode | Total run duration (min) |
|---|---|---|---|---|---|---|---|---|
| A1 | 2 | 593 | 660 | 2 | 16.5 | 60 | Continuous | 60 |
| A2 | 2.1 | 593 | 669 | 3.36 | 28.1 | 60 | Continuous | 60 |
| A3 | 1.8 | 593 | 642 | 0.44 | 3.5 | 60 | Continuous | 60 |
| A4 | 0.85 | 594 | 657 | 2.01 | 16.5 | 60 | Sequenced | 120 |
| A5 | 1.5 | 588 | 650 | 1 | 13.6 | 100 | Continuous | 100 |
| A6 | 2.35 | 544 | 657 | 2.01 | 16.5 | 60 | Continuous | 60 |
| A7 | 2.25 | 584 | 660 | 2 | 16.5 | 60 | Sequenced | 120 |
| A8 | 0.85 | 501 | 657 | 2.01 | 16.5 | 60 | Continuous | 60 |
| R1 | 1.95 | 580 | 609 | 0.4 | 3.58 | 70 | Continuous | 70 |
| R2 | 3.7 | 588 | 595 | 0.43 | 3.75 | 70 | Continuous | 70 |
| R3 | 2 | 586 | 620 | 0.17 | 1.32 | 60 | Continuous | 60 |
| R4 | 5.6 | 564 | 627 | 0.18 | 1.43 | 60 | Continuous | 60 |
| R5 | 2 | 588 | 623 | 0.18 | 2.77 | 120 | Continuous | 120 |

**Table 2**
Experimental results.

| Run | Temperature gradient (°C/cm) at the end of the runs | Vol. % of $H_2$ | Weight of Si deposited (from the vol. % of $H_2$) (g) | Theoretical thickness of deposition (nm) | Deposition rate (g/min) | Deposition rate (nm/h) | Elutriation (wt. %) |
|---|---|---|---|---|---|---|---|
| A1 | 2.75 | 3.98 | 16.4 | 5.2 | 0.27 | 5.2 | 6.94 |
| A2 | 1.3 | 6.37 | 26.6 | 8.2 | 0.44 | 8.2 | 7.56 |
| A3 | 1.35 | 0.86 | 3.45 | 1.1 | 0.05 | 1.1 | 8.66 |
| A4 | 1.95 | 4.15 | 17.1 | 5.5 | 0.284 | 5.5 | 9.17 |
| A5 | 1.1 | 1.99 | 13.5 | 4.4 | 0.135 | 4.4 | 9 |
| A6 | 2.35 | 3.86 | 15.8 | 5.1 | 0.264 | 5.1 | 11 |
| A7 | 1.1 | 4.16 | 17.1 | 5.5 | 0.284 | 5.5 | 10.2 |
| A8 | 0.7 | 3.99 | 16.4 | 5.3 | 0.273 | 5.3 | 9.98 |
| R1 | 3.2 | 0.79 | 3.52 | 1.3 | 0.05 | 1.1 | 28.4 |
| R2 | 2.35 | 0.88 | 3.83 | 1.4 | 0.055 | 1.2 | 25.3 |
| R3 | 1.35 | 0.33 | 1.28 | 0.5 | 0.02 | 0.47 | 24.4 |
| R4 | 4.6 | 0.41 | 1.57 | 0.7 | 0.026 | 0.7 | 32.7 |
| R5 | 2.2 | 0.37 | 2.8 | 1.2 | 0.023 | 0.58 | 38.9 |

A6 and A8, performed for the same total mass of silicon injected. Runs A1, A2 and A3 were conducted at the same mean temperature but for different total amounts of silicon injected. And repeatability of experiments was checked with runs A4/A7 and R1/R2, performed in very close conditions.

The mass of silicon deposited could not be measured by weighing because of the low amount of injected silane and of elutriation. The deposition rate and a theoretical thickness of deposition were deduced from the hydrogen concentration of the outlet gases. The theoretical thickness was calculated assuming that the particles were spherical and the deposition was uniform. Elutriation was measured by weighing the bed at the beginning and at the end of the deposition, and by considering the additional mass due to silicon deposition. The cooling of the region below the distributor was responsible for significant thermal gradients along the bed. They were slightly higher for rutile $TiO_2$ runs than for anatase ones, probably because of less optimized fluidization conditions for rutile powders, leading to a more agglomerated state of powders, as explained below.

The powders before and after CVD treatment were analyzed as follows:

- Laser scattering size analyses of particles after air-dispersion under 4 bars were performed with a MasterSizer2000 Malvern setup. Each measurement corresponds to an average value calculated over 3 runs.
- The powder morphology was observed by Scanning Electron Microscopy (SEM) on a LEO 435 VP, by Field Effect Gun SEM (FEG SEM) using a JEOL 6700S and also by Transmission Electron Microscopy (TEM) on a Philips CM20 setup.
- The chemical composition of the depositions has been studied by Raman spectroscopy, using a Labram HR800 from Jobin et Yvon setup equipped with a He/Ne laser, and by Infra-Red (IR) spectroscopy on a PerkinElmer Series 100 spectrometer in transmission, after dispersion of powders in KBr.

## 3. Results and discussion

Results are detailed in Table 2. The conversion rate of silane was always of 100%, thanks to the low inlet percentage of silane used and to the high specific surface area of powders. Some reproducibility runs (A4, A7 and R1, R2) have been performed as detailed in Tables 1 and 2, showing that the conditions of deposition were conveniently mastered and led to reproducible results. The theoretical thickness of deposition was close to 1 nm for the rutile particles and has been increased to 5 nm in average for the anatase powders, to better detect silicon. The corresponding deposition rates were very low, close to 0.03 g/min for the rutile particles, and ten times higher (0.3 g/min) for the anatase ones. Thermal gradients were often higher at the end of the runs than before deposition, because of some agglomeration phenomena, as detailed below. For anatase runs, elutriation was proportional to the run duration and remained lower than 11 wt.%. Elutriation was much higher for rutile runs, since it reaches in average 30 wt.%. This difference is probably due to a specific agglomeration state of particles during fluidization, which is very different between rutile and anatase particles.

### 3.1. Granulometry

#### 3.1.1. Sieving

After CVD runs, the whole powders were under the form of agglomerates. The results obtained by sieving are detailed in Table 3 and in Fig. 1.

For all runs, the diameters of agglomerates are mainly between 100 and 500 μm. The mass fraction of agglomerates comprised between 700 and 900 μm is always very low. For some runs, especially using rutile $TiO_2$, agglomerates of diameter higher than 1 mm are present; they are much harder and mechanically resistant than the rest of the powders. They have always been found at the bottom of the bed, near the distributor, so near the silane entrance.

If we focus on the results obtained with anatase $TiO_2$, the presence of agglomerates of diameter higher than 1 mm is very low; it is even equal to zero for runs A2, A5, A6, A7 and A8. Their average mass fraction on the whole runs is lower than 1.6%. Such big agglomerates are more present for runs A1, A3 and A4. There is no clear influ-

**Table 3**
Sieving results.

| Run | Proportion of agglomerates of size higher than 1 mm (% of the total mass) | Mean diameter of agglomerates (μm) |
|---|---|---|
| A1 | 8.6 | 405 |
| A2 | 0.12 | 330 |
| A3 | 1.47 | 392 |
| A4 | 3.26 | 349 |
| A5 | 0.02 | 409 |
| A6 | 0.24 | 356 |
| A7 | 0.025 | 311 |
| A8 | 0.05 | 313 |
| A9 | 0.35 | 326 |
| Average | 1.57 | 355 |
| Run | Proportion of agglomerates of size higher than 1 mm (% of the total mass) | Mean diameter of agglomerates (μm) |
| R1 | 12.2 | 375 |
| R2 | 14.9 | 409 |
| R3 | 17.2 | 396 |
| R4 | 8.9 | 371 |
| R5 | 7 | 305 |
| Average | 12 | 371 |

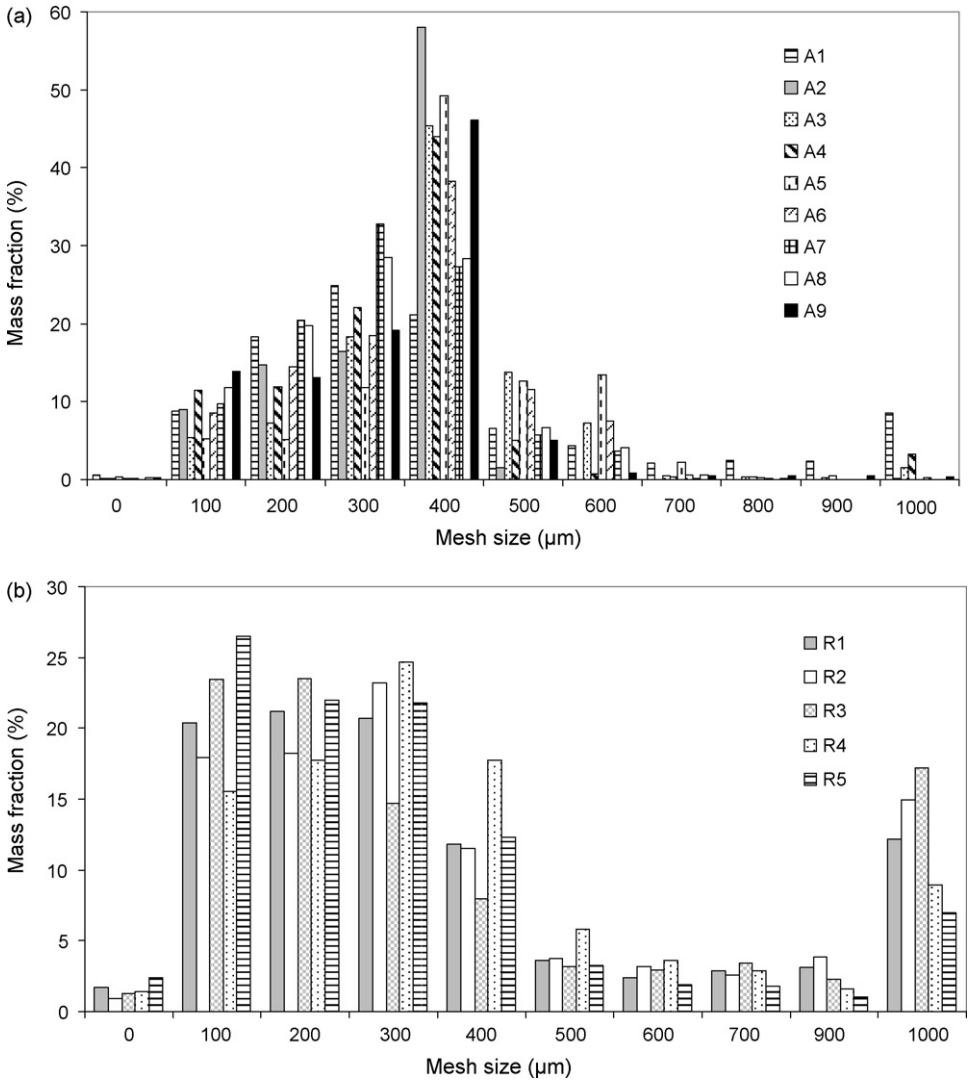


**Fig. 1.** Size distribution of powders after CVD measured by sieving for (a) anatase $TiO_2$ runs and (b) rutile $TiO_2$ runs.

ence of the deposition conditions on their formation. For instance, no trend can be found for runs A8, A6 and A7 performed with 2% of silane in entrance at increasing temperature, or for runs A3, A1 and A2 performed near 590 °C at increasing inlet concentration of silane. For the conditions tested, the formation of agglomerates mainly depends on the fluidization conditions, and in particular on the existence of a very poorly fluidized zone near the bottom of the bed. The use of sequential injections of silane has not provided a clear minimization of agglomerates, due to the bad results of run A4. However, if we compare runs A1 and A7 performed in the same conditions except the sequential silane injection for A7, the results are clearly better for the latter. A perspective to this work will then be to continue the study of sequential deposition.

If we focus now on rutile results, the size distribution is more spread than for anatase, and the percentage of big agglomerates is much more important than for anatase: it represents till 17.2% of the bed mass, with an average of 12% for the whole runs. These bad results are probably due to the fact that the FB hydrodynamics of the rutile powders could not been optimized as far as for anatase particles.

*3.1.2. Laser granulometry*

It is worth noting that the agglomerates of diameter higher than 1 mm have been removed of the whole samples analyzed because such sizes are above the range of diameters covered by the granulometer. Of course, for the runs for which such agglomerates were not present (runs A2, A5, A6, A7 and A8), the analyses concern the whole powders.

For anatase $TiO_2$, Fig. 2(a) and (b) shows that two distinct populations appear concerning the volumic fractions, one centered on the initial diameter of particles, the other around 100 µm. Agglomerates of higher diameter are no more visible, probably because they have been broken up by the high air pressure (4 bar) applied during the analyses. The size distributions of particles seem to be independent of the deposition conditions, since the spectra are close to each other. When analyzing the size distribution in number (Fig. 2(c) and (d)), for all runs, the original granulometry is preserved, indicating that the agglomerates observed in the analyses in volume only represent a low percentage in mass.

If these agglomeration results are put in regards with the corresponding thermal profiles, the temperature close to the distributor decreased all along deposition for run A1 [20]. A similar behavior was observed for run A4 for which 3.3 wt.% of millimetric agglomerates have been formed, whereas a good thermal stability has been obtained for run A3 (1.5 wt.% of millimetric agglomerates). It can then be inferred that the formation of less than 2% in weight of millimetric agglomerates does not disturb the process when using the anatase powders.

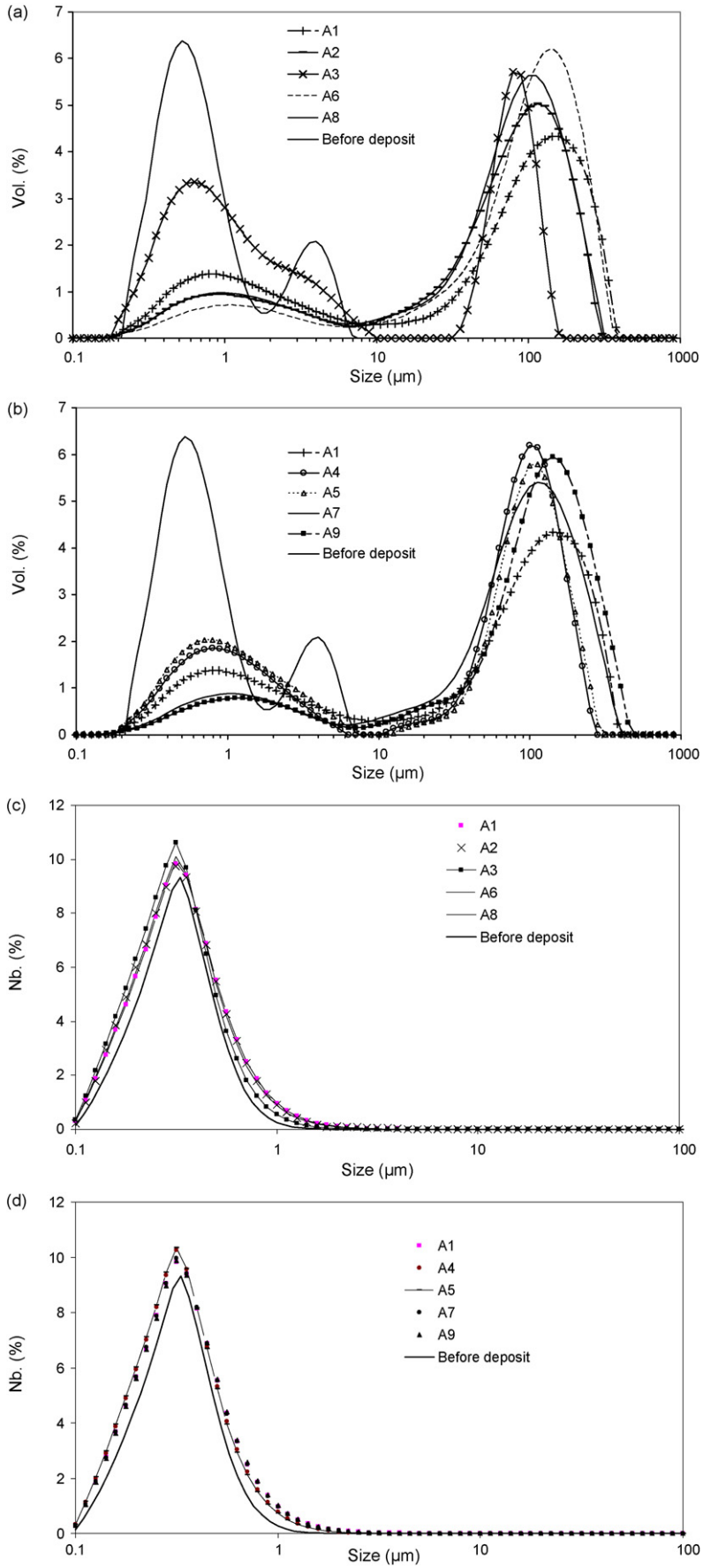


**Fig. 2.** Size distribution of anatase $TiO_2$ powders before and after CVD measured by laser granulometry, presented in (a) and (b) volumic fractions, (c) and (d) number fractions.

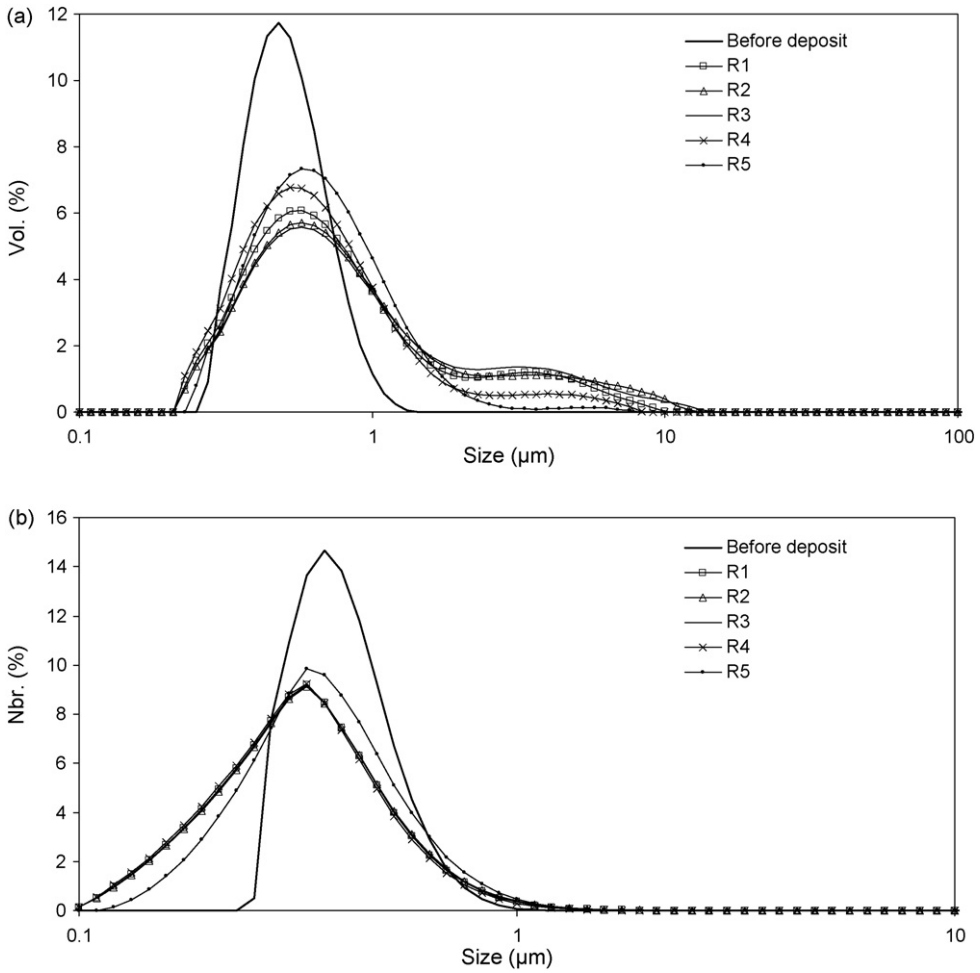


**Fig. 3.** Size distribution of rutile $TiO_2$ powders before and after CVD measured by laser granulometry, presented in (a) volumic fractions, (b) number fractions.

For rutile $TiO_2$ samples, as previously said, roughly 10 wt.% of the bed weight corresponds to big agglomerates; they have been removed of the samples before laser granulometry analysis. Let us note that these big agglomerates can easily be separated of the rest of the particles.

Fig. 3(a) shows that the whole volume distributions of the remaining powders are close to the initial one. A second population appears for a mean diameter close to 5 μm, which probably corresponds to mechanically resistant small agglomerates. When analyzing the distribution in number (Fig. 3(b)), these agglomerates are no more present, indicating that their mass percentage is low. The size distributions in number are more spread due to the presence of smaller particles than the initial rutile powders. We will propose an explanation to this fines formation in Section 3.2.

Comparison of results between anatase and rutile confirms the fact that the agglomeration state cannot be explained by the CVD conditions. In particular, the deposition rate was ten times higher for the anatase powders than for the rutile ones, and despite this, the agglomeration phenomenon was much more intense for the rutile powders.

To have a better insight of the agglomeration mechanisms, the whole particles, before and after CVD, have been analyzed by BET and helium pycnometry. After anatase $TiO_2$ runs, the mean specific surface area is of 11.6 $m^2/g$ and remains quite identical from one run to another (for an initial value of 10.07 $m^2/g$). This indicates that the agglomerates are porous and that no dense deposition occurs around the agglomerates, allowing keeping the original specific surface area. This explains the fact that most of them were disintegrated during granulometry analysis.

For rutile $TiO_2$ runs, the mean specific surface area of powders after CVD is of 11.4 $m^2/g$, to be compared to 16.3 $m^2/g$ before treatment. This decrease indicates that a part of the agglomerates has been densified by deposition, which is logical regarding the relative high proportion of mechanically resistant agglomerates formed.

Anatase agglomerates were probably more dynamic during fluidization than rutile ones. As a consequence, they have been much less densified by CVD.

### 3.2. TEM and SEM analyses

Fig. 4 presents some representative TEM results before and after CVD on anatase $TiO_2$. Silicon deposition clearly appears as nanodots on the surface of particles. No interparticle bridge has been detected; deposition seems to occur around each individual grain.

For the whole anatase runs, a good uniformity of the treatment has been evidenced between samples taken at various levels into the bed (at the top part and at 15 cm above the distributor), as seen in Fig. 4(e) and (f). This indicates a good axial circulation of powders into the bed during runs, due to a satisfactory quality of fluidization.

However, it clearly appears that the depositions are not continuous around each grain and that some parts of the grains are more covered than others. Local defects on the grains surface and/or ephemeral agglomeration of grains could explain this result.

The deposition thickness has been evaluated from these images as comprised between 8 and 10 nm. These values are slightly higher

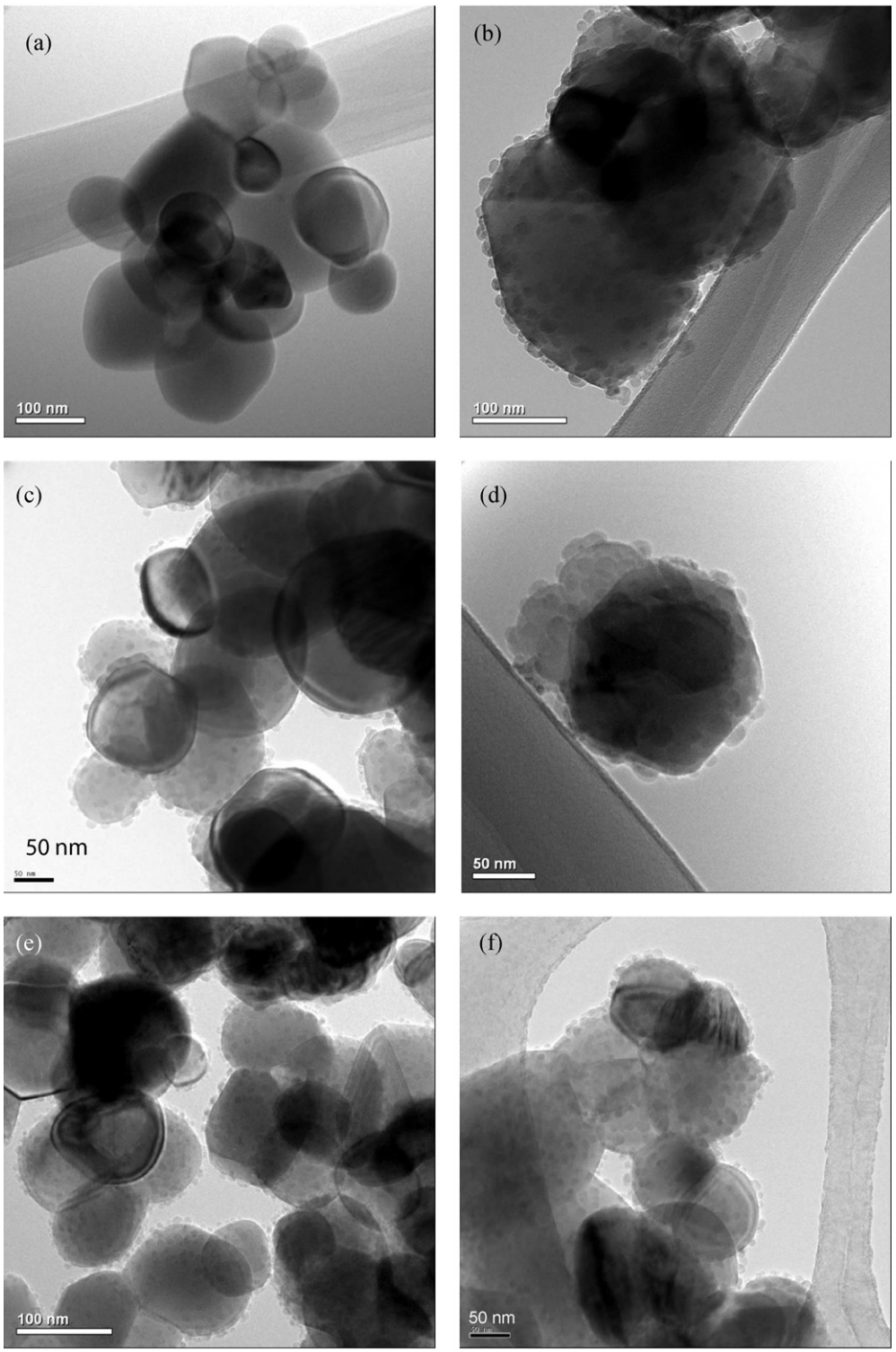


**Fig. 4.** TEM analyses of anatase $TiO_2$ powders (a) before CVD and after CVD for (b) run A2, (c) run A3, (d) run A6, (e) run A4 (middle of the bed), and (f) run A4 (top of the bed).

than the theoretical ones (close to 5 nm, see Table 2), probably because of the discontinuity of the deposition. However, the difference is quite low, which demonstrates that deposition occurred on the whole powders. The fact to have worked with a very low deposition rate of silicon has certainly favored the diffusion of the reactive gas up to the centre of the agglomerates.

From a qualitative point of view, without being statistical, it appeared by TEM that the most uniformly treated powders were those of run A4 and A7 using a sequential injection of silane.

For rutile $TiO_2$, TEM observations have not allowed to evidence the presence of deposition due to the low weights of silicon deposited and to the bad interface quality of these rutile powders [20]. These depositions have however been observed by FEG SEM as illustrated in Fig. 5. Silicon nodules clearly appear on the surface of the grains, but treatments are not uniform: some parts of the grains seem to be not covered by silicon. Moreover, interparticle filaments are present which could be at the origin of the agglomerates formation. These filaments could also easily be broken during fluidization

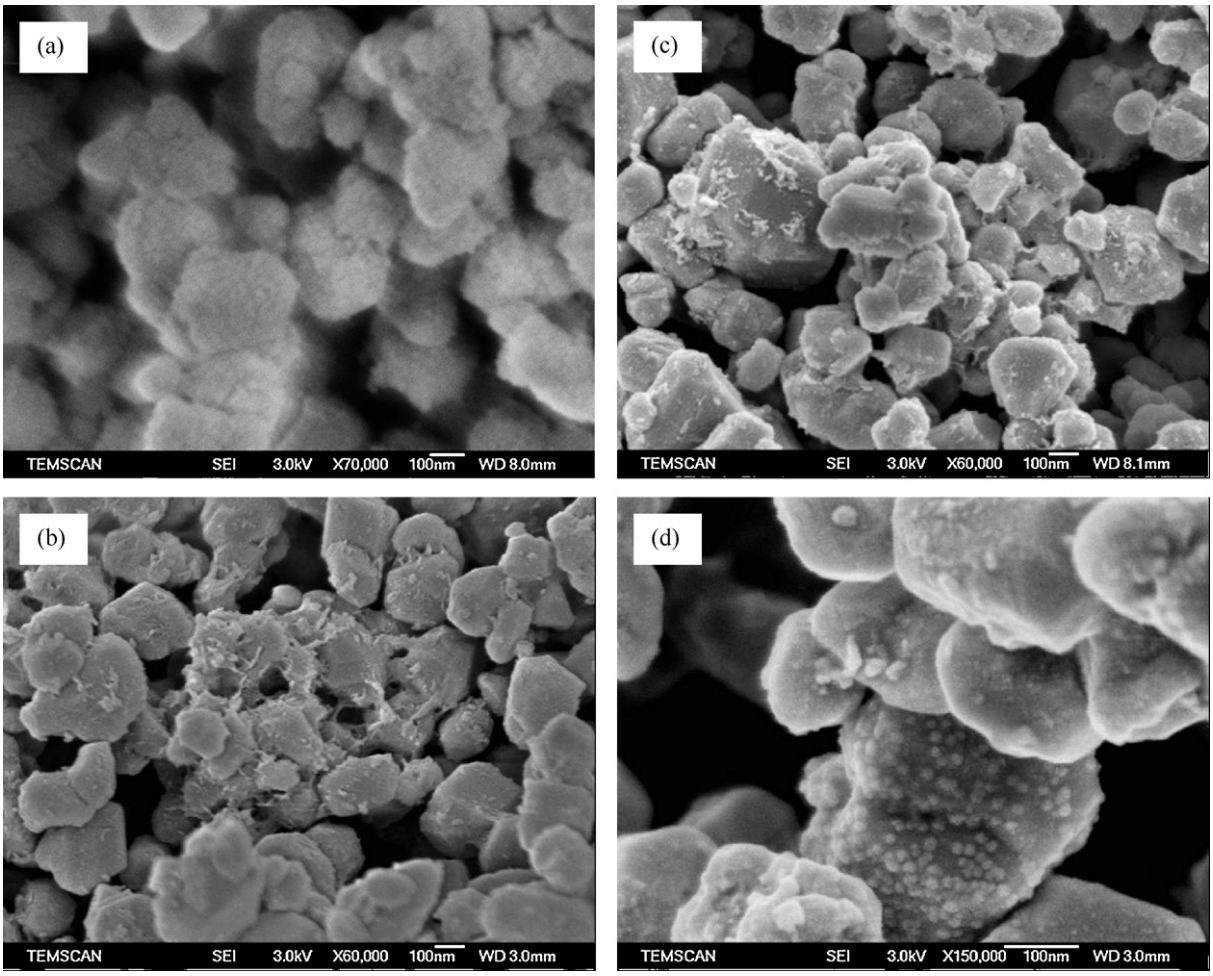


**Fig. 5.** FEG SEM views of rutile $TiO_2$ powders (a) before CVD, and (b) to (d) after run R2.

and handling of the treated powders and then could correspond to the population of fines observed by laser granulometry as reported in Section 3.1.2. The formation mechanism of these filaments is difficult to explain. But these SEM results confirm that the rutile particles form more compact agglomerates than the anatase ones, and that the individual grains in the agglomerates were probably more static during fluidization.

### 3.3. Raman and Infra-red spectroscopy

Si deposition on the $TiO_2$ powders resulted in a marked modification of their color, from white before deposition to more or less dark grey after treatment. We tried to identify the nature of the deposits, and possibly of their interaction with the substrate, by vibrational spectroscopies. We have only studied here the anatase powders.

Raman investigation has been performed with a microprobe attachment, the sample being simply sprinkled on a glass plate. The volume investigated is about 1 $\mu m^3$, which corresponds to a few anatase particles. This technique allows having an idea upon the homogeneity in terms of composition and structure of the powders at this spatial resolution.

For runs A2 and A5, heterogeneities at the scale of the probe have been evidenced. For each zone investigated, the Raman spectrum of titania (described below) is observed. However for some zones, it super imposes to that of amorphous silicon, which has been clearly identified by comparison with data of Zwick and Carles [21], Mahon et al. [22] or Zhang et al. [23].

These observations confirm that silicon has not been deposited uniformly on the $TiO_2$ grains for these runs.

For all other runs, the Raman spectrum of silicon does not appear and no compositional heterogeneity has been detected. So, even if Si nanodots have been clearly seen by TEM for these runs, they are probably too small to be detected by Raman scattering.

However, additional information can be extracted since a chemical modification of the substrate during deposition has been evidenced. Except for runs A2 and A5 described above, the only spectrum observed for all investigated zones is shown in Fig. 6, together with that of $TiO_2$ before deposition. Before FBCVD, a very intense and sharp peak at 142 $cm^{-1}$, and some well-defined and less intense components listed in Table 4 are observed. There is a good agreement between our observations and those reported previously for anatase (natural or synthetic) crystals or for anatase powders [24–26]. The assignment of the vibration modes given in

**Table 4**
Observed Raman shifts and their assignment according to Balachadran and Eror [26].

| Vibration mode | $TiO_2$ anatase initial observed shift ($cm^{-1}$) | $TiO_2$ anatase after FBCVD observed shift ($cm^{-1}$) |
|---|---|---|
| $E_g$ | 142 | 146–150 |
| $E_g$ | 196 | 196 |
| Overtone or defects | 320 | 320 |
| $B_{1g}$ | 397 | 390–392 |
| $A_{1g}$, $B_{1g}$ | 514 | 506 |
| $E_g$ | 638 | 626–629 |
| Overtone | 800 | 800 |

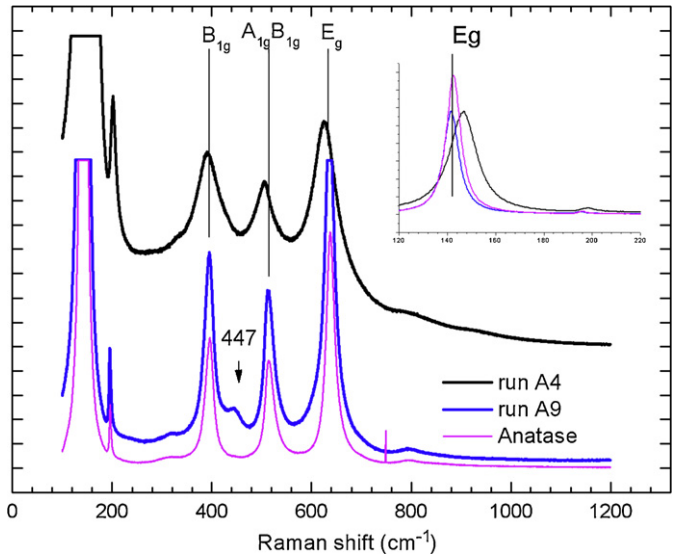


**Fig. 6.** Raman spectroscopy of anatase $TiO_2$ powders before deposition, after run A4 and after run A9 (annealing under air of run A4). Assignments refer to vibration modes of anatase; at 447 $cm^{-1}$: Raman mode of rutile.

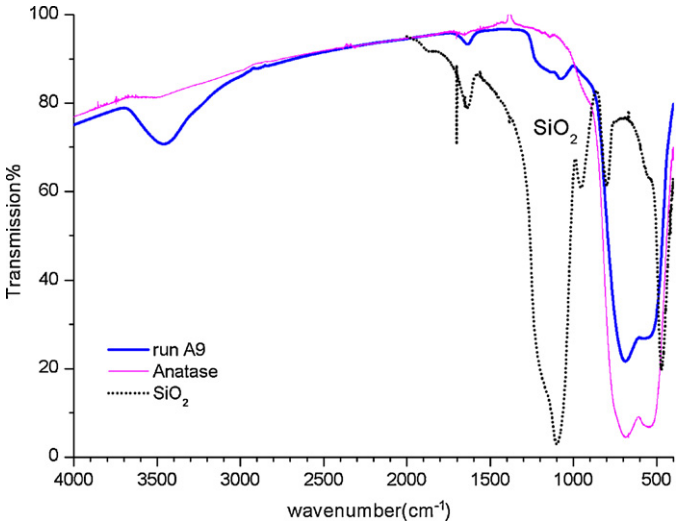


**Fig. 7.** IR transmission spectra of anatase before deposition and after run A9. The IR spectrum of silica powders is given as a reference.

Table 4 has been done in Refs. [24,25]. In the spectrum recorded after run A4 (the observed Raman shifts are given in Table 4), the components are more or less shifted with respect to $TiO_2$, specially the first $E_g$ mode towards higher wave numbers, and they are broader. Parker and Siegel [27] have linked unambiguously the decrease of the O/Ti ratio in anatase with the shift towards higher wavenumbers of the strongest $E_g$ anatase mode (142 $cm^{-1}$) and with the increase of its full-width at half-maximum, all features we observed after FBCVD on anatase. We may thus conclude safely that the anatase powder has been partially reduced into $TiO_{2-x}$ by the formation of hydrogen during the CVD from $SiH_4$.

An annealing under air in the FB process at 600 °C during 2 h has been performed on the powder formed after run A4, in order to re-establish the $TiO_2$ stoichiometry of the substrate and at the same time to oxidize the silicon deposition (run A9). After this oxidizing treatment, the powder has recovered a white, lightly ochre, color. The same Raman spectrum (run A9 in Fig. 6) has been recorded for all parts of the sample investigated. The measured Raman shifts are in exact coincidence with those of $TiO_2$ before CVD and all the components are significantly narrower compared to A4: this proves that the stoichiometric $TiO_2$ anatase phase has been recovered by the oxidizing annealing. Compared to the spectrum of anatase, there is only one important difference: a band at 447 $cm^{-1}$ is observed. This band may be assigned to the $E_g$ mode of rutile according to [26]; a transformation of anatase into rutile has probably been initiated during the oxidizing annealing.

The amorphous Si, which has a very good Raman scattering efficiency, has not been detected in sample A4, certainly because the deposited nanodots are too thin. So, there was little chance to observe the response of $SiO_2$ in the oxidized sample. But the presence of silica after the oxidizing treatment has been well confirmed by FTIR. In Fig. 7 are displayed the IR spectra of $TiO_2$ anatase before deposition, and after run A9 (oxidizing annealing of run A4). The more intense absorptions in the 500–750 $cm^{-1}$ wave number range are those of $TiO_2$ and the new bands observed in the range 1000–1250 $cm^{-1}$ for run A9 denote unambiguously the presence of amorphous silica (the IR spectrum of a reference silica powder is also displayed). The other bands at 1600 and 3400 $cm^{-1}$ are due to adsorbed water. It can then be concluded that after the oxidizing annealing, grains of stoichiometric $TiO_2$ are coated by silica nanodots.

## 4. Conclusions

Silicon nanodots have been deposited on submicronic $TiO_2$ particles in a vibrated fluidized bed CVD reactor from silane $SiH_4$ highly diluted in nitrogen. Various temperatures, deposition durations and silane inlet concentrations have been studied, but always chosen in a range involving very low deposition rates.

After deposition, powders are under the form of micronic agglomerates. The agglomeration intensity mainly depends on the vibro fluidization conditions and not on the CVD parameters, at least in the operating range tested.

The best results have been obtained for the anatase $TiO_2$ powders for which the best optimization of the fluidization hydrodynamics could be achieved. For these anatase powders, agglomerates are porous and deposition occurs under the form of silicon nanodots. These nanodots seem to be deposited uniformly on the whole powders and conformally around each grain, even if not always continuously. According to Raman spectroscopy spectra, the $TiO_2$ powders have been partially reduced into $TiO_{2-x}$ during the treatment, leading to a dark grey color after CVD. The original white color has been recovered after annealing under air in the fluidized bed, and IR spectroscopy indicates that the deposited silicon nanodots are at least partly oxidized into $SiO_2$ after this annealing.

A perspective of this work will be to study more deeply the sequential injection of silane, to try to improve the continuity of deposition around each grain. Another perspective could be to operate with other precursors (for instance TEOS, tetra-ethoxy-silane $Si(OC_2H_5)_4$), to directly deposit silicon dioxide nanodots without modifying the $TiO_2$ structure.

## Acknowledgements

The authors acknowledge M. Molinier and E. Prévot from LGC/INPT for technical support and C. Routaboul from Université Paul Sabatier, for recording and discussing the Raman spectra. This project has been supported by the French Agence Nationale de la Recherche - Réseau National Matériaux et Procédés and by the Midi-Pyrénées region.

## References

[1] M. Maeda, T. Watanabe, Surf. Coatings Technol. 201 (2007) 9309–9313 (and references therein).

[2] J.R. Scheffe, A. Frances, D.M. King, X. Liang, B.A. Branch, A.S. Cavanagh, S.M. George, A.W. Weimer, Thin Solid Films 517 (2009) 1874–1879.
[3] R. Nauman d'Alnoncourt, M. Becker, J. Sekulic, R.A. Fisher, M. Muhler, Surf. Coatings Technol. 201 (2007) 9035–9039.
[4] G.S. Czok, J. Werther, Powder Technol. 162 (2006) 100–110.
[5] D. Chaliampalas, G. Vourlias, N. Pistofidis, E. Pavlidou, A. Stergiou, G. Stergioudis, E.K. Polychroniadis, D. Tsipas, Mater. Lett. 61 (2007) 223–226.
[6] J. Perez-Mariano, K.H. Lau, E. Alvarez, R. Malhotra, M. Hornbostel, Mater. Chem. Phys. 112 (2008) 180.
[7] D Geldart, Powder Technol. 7 (1973) 285–292.
[8] A. Dutta, L.V. Dullea, AIChE. Symp. Ser. 87 (281) (1991) 38–46.
[9] T. Zhou, H. Li, Powder Technol. 102 (1999) 215–220.
[10] J. Kim, G.Y. Han, Powder Technol. 166 (2006) 113–122.
[11] J.R. Wank, S.M. George, A.W. Weimer, Powder Technol. 121 (2001) 195–204.
[12] S. Alavi, B. Caussat, Powder Technol. 157 (2005) 114–120.
[13] C. Xu, J. Zhu, Powder Technol. 161 (2006) 135–144 (and references therein).
[14] S. Morooka, K. Kusakabe, A. Kobata, in: G.R. Grace, L.W. Shemilt, M.A. Bergougnou (Eds.), Fluidization VI, AIChE, New York, 1989, p. 359.
[15] C. Li, B. Hua, Thin Solid Films 310 (1997) 238–243.
[16] L.F. Hakim, S.M. George, A.W. Weimer, Nanotechnology 16 (2005) 2375–2381.
[17] D.M. King, J.A. Spencer II, X. Liang, L.F. Hakim, A.W. Weimer, Surf. Coatings Technol. 210 (2007) 9163–9171.
[18] L. Cadoret, N. Reuge, S. Pannala, M. Syamlal, C. Rossignol, J. Dexpert-Ghys, C. Coufort, B. Caussat, Surf. Coatings Technol. 201 (2007) 8919–8923.
[19] D. Kunii, O. Levenspiel, Fluidization Engineering, 2nd ed., J. Wiley and Sons, New York, 1991.
[20] L. Cadoret, PhD thesis, INP Toulouse, France, 2007.
[21] A. Zwick, R. Carles, Phys. Rev. B 48 (9) (1993) 6024–6032.
[22] D.C. Mahon, P.J. Mahon, D.C. Creagh, Nucl. Instrum. Methods Phys. Res. A580 (2007) 430–433.
[23] S. Zhang, X. Liao, L. Raniero, E. Fortunato, Y. Xu, G. Kong, H. Aguas, I. Ferreira, R. Martins, Solar Energy Mater. Solar Cells 90 (2006) 3001–3008.
[24] I.R. Beattie, T.R. Gilson, Proc. Royal Soc. London A307 (1968) 407–429.
[25] T. Ohsaka, S. Yamaoka, O. Shimomura, Solid State Commun. 30 (1979) 345–347.
[26] U. Balachadran, N.G. Eror, J. Solid State Chem. 42 (3) (1982) 276–282.
[27] J.C. Parker, R.W. Siegel, Appl. Phys. Lett. 57 (9) (1990) 943–945.